DESIGN AND TESTING OF SPIRAL CUTTER TOOTH TYPE FARMLAND STONE PICKER
/
螺旋刀齿式农田捡石机的设计与试验

Jia ZHANG[1,2], Heng QU [2], Ping XIAO [1], Shaoteng MA [1,2], Weisong ZHAO[3,4*]
[1]School of Mechanical and Electrical Engineering, Xinjiang Institute of Engineering, Urumqi, Xinjiang / China
[2] School of Mechanical and Electrical Engineering, Xinjiang Agricultural University, Urumqi, Xinjiang / China
[3] Western Agricultural Research Center, Chinese Academy of Agricultural Sciences, Changji, Xinjiang / China
[4] Nanjing Institute of Agricultural Mechanization, Ministry of Agriculture and Rural Affairs, Nanjing / China
Tel: +8613579297197; E-mail: zj34@xjie.edu.cn
Corresponding author: Weisong Zhao
DOI: https://doi.org/10.35633/inmateh-75-74

Keywords: *agricultural stone picker, spiral cutter drum, EDEM, soil trench test*

ABSTRACT
This study aimed to solve the inefficiency and high-energy-consumption problems of current agricultural stone pickers. It introduced a novel spiral cutter tooth design. Dynamic and kinematic analyses determined the key components' parameters and performance-influencing factors. With EDEM software, discrete element simulations using a three-factor, five-level quadratic regression orthogonal design were carried out. Stone-picking efficiency and power consumption were the evaluation metrics. Regression analysis and significance tests clarified the impact of forward speed, drum speed, and tilt angle. Multi - objective optimization of the regression model found the optimal parameters: 0.18 m/s forward speed, 260 rpm drum speed, and 30° tilt angle. Field tests with this setup achieved a 93.71% stone-picking rate and 4.63 kW stable power, validating the design's effectiveness. These results offer a theoretical basis and reference for stone picker design and optimization.

摘要
针对现有农田捡石机捡石效率低，消耗功率大等问题，提出了一种螺旋刀齿式农田捡石机，通过动力学和运动学分析，确定了关键部件的结构参数和运动参数范围，以及影响工作性能的主要因素。利用 EDEM 软件开展了离散元仿真试验，采用三因素五水平二次回归正交旋转中心组合试验方法，以捡石效率和消耗功率为评价指标，对机具前进速度、螺旋刀辊转速和螺旋刀辊侧倾角进行回归分析和显著性检验，明确了各因素对评价指标的影响及主次顺序，通过对回归模型进行多目标函数优化求解，得出最佳参数组合为机具前进速度 0.18 m/s、螺旋刀辊转速 260 r/min、螺旋刀辊侧倾角 30°。使用最佳参数组合进行了土槽试验，试验结果表明：捡石效率为 93.71%，稳定作业时的功率为 4.63 kW，螺旋刀齿式捡石机作业稳定，满足农田捡石作业要求。

INTRODUCTION
Arable land forms the cornerstone of agricultural development, with soil quality enhancement being paramount for sustainable farming practices *(Zhan et al., 2023)*. In northwestern China's newly developed Gobi farmlands, stony soils present a critical challenge. Elevated stone content restricts root proliferation, exacerbates soil desiccation, reduces seed germination rates, and ultimately compromises crop yields *(Yu et al., 2007; Zhang et al., 2024)*. Furthermore, stone interference during mechanized operations accelerates equipment wear and impedes agricultural modernization.

Current stone removal strategies predominantly employ mechanical methods over manual collection *(Li et al., 2024; Bu et al., 2022)*. Existing machinery—including comb-tooth shovels, tooth rakes, and shovel-chain systems—has been extensively studied. For example, Yu et al. developed a chain-tooth stone picker demonstrating high efficiency through dynamic analysis of soil-tool interactions, though limited by shallow excavation depth *(Yu et al., 2007)*. *Ma et al. (2007)* achieved shallow-layer stone removal (≤100 mm) using a wheel-tooth rake, yet faced challenges of excessive energy consumption and suboptimal collection rates. *Niu et al., (2007),* advanced the field with a shovel-sieve design, employing discrete element modeling to analyze stone-soil separation dynamics. While functional, these systems universally exhibit energy inefficiency and inconsistent performance.

Jia Zhang, Assoc. Prof; Heng Qu, Student; Ping Xiao, Assoc. Prof; Shaoteng Ma, Lecturer; Weisong Zhao, Lecturer

To address these limitations, a novel spiral cutter tooth stone picker is introduced. Through kinematic analysis of stone-cutter interactions, critical operational parameters governing collection efficiency are identified. EDEM simulations and field trials validate the optimized design, demonstrating enhanced performance while reducing power demands. This work establishes a theoretical framework for advancing stone-picking technology, offering practical insights for agricultural equipment innovation.

MATERIALS AND METHODS

Overall structure and working principle

The spiral cutter tooth stone picker for agricultural fields primarily comprises a frame, gearbox, spiral cutter rollers, cutter teeth, and deflector plates. The spiral cutter rollers are symmetrically mounted on the frame at specific angles on either side, and the cutter teeth are arranged in a double helical line extending outward. The structure is illustrated in Fig 1.

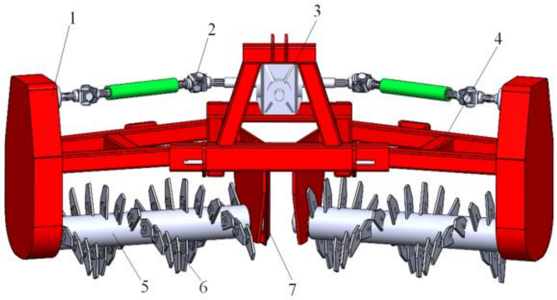

Fig. 1 – Schematic diagram of the overall structure

1.transmission device; 2. universal shaft; 3. gearbox; 4. frame; 5. spiral cutter rollers; 6. cutter teeth; 7. deflector plate

During operation, the machine connects to the tractor via a three-point hitch. The tractor provides power that is transmitted through the gearbox to the universal shaft and then through the internal transmission chains of the drive devices on both sides to the spiral blade roller. The rotational speed of the spiral blade roller aligns with the forward direction of the machine, effectively lifting stones from the surface and from certain soil depths. The lifted stones are conveyed toward the center, where the inner guide plates on the frame align them into rows, completing the stone-picking process. This machine not only picks stones but also tills and effectively loosens the soil. A schematic of the stone picker operation is shown in Fig. 2, and the main technical parameters are listed in Table 1.

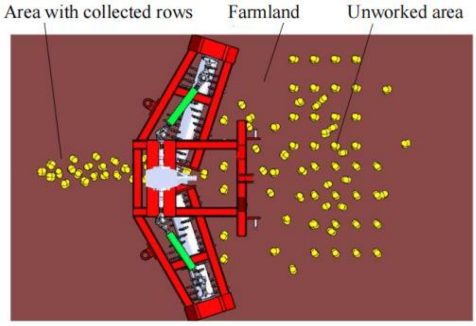

Fig. 2 – Schematic diagram of the operating principle of the stone picker

Table 1

Main technical parameters of the stone picker

Parameter	Value
Connection type	Suspension type
Overall dimensions (length×width×height) (mm)	2500×1105×1210
Working width (mm)	2100
Working depth (mm)	55
Spiral blade roller speed (r/min)	150~350
Traction power (kW)	≥40

Tooth structure design

The installation type of the teeth significantly affects the performance of the stone picker. Depending on the angle between the tangent at the point of contact between the tooth blade and the tooth shaft, the teeth can be classified as radial, forward-leaning, or backward-leaning. A force analysis is conducted at initial contact with the stone and when the stone is lifted off the ground for various tooth types to compare their effectiveness in stone picking. The force analysis for the three types of teeth is illustrated in Fig 3.

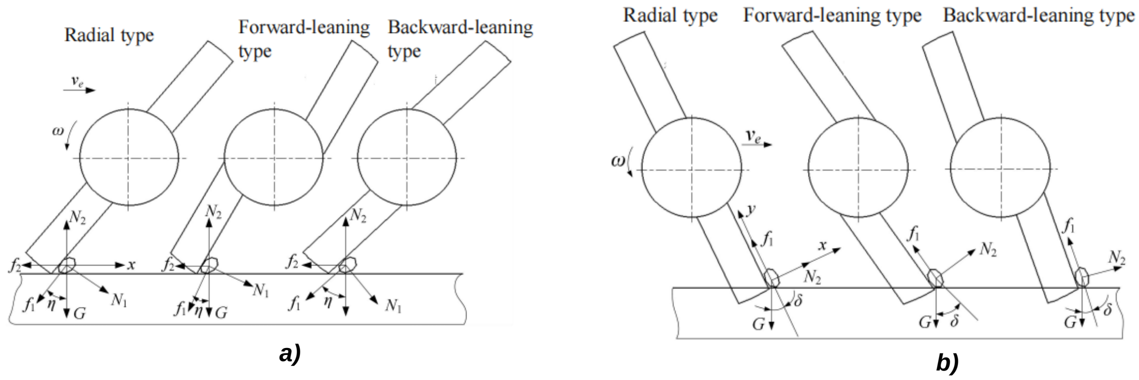

Fig. 3 – Force analysis of stones during operation

a) Force analysis of the stone at initial contact with the tooth; b) Force analysis of the stone during lifting by the tooth

As shown in Figure 3a, a coordinate system is established with the center of the stone as the origin, where the *x*-axis is parallel to the ground and the y-axis is perpendicular to it. When the tooth contacts the stone, there is no vertical movement relative to the ground; instead, the stone primarily undergoes horizontal displacement. The velocity along the x-axis is determined by the horizontal resultant force. The expression for this resultant force is given by:

$$F_{xa} = N_1 \cos\eta - f_1 \sin\eta - f_2 \quad (1)$$

where:

F_{xa} is the resultant force of the tooth in the horizontal direction, [N]; N_1 is the support force exerted by the tooth on the rock, [N]; η is the angle of entry into the soil, [°]; f_1 is the frictional force of the tooth on the rock, [N]; f_2 is the frictional force of the ground on the rock, [N]; G is the gravitational force of the rock, [N].

The derivative of equation (1) yields:

$$F'_{xa} = -N_1 \sin\eta - f_1 \cos\eta \quad (2)$$

where:

$$\eta < \pi/2 \quad (3)$$

This resultant force is derived from equations (2) to (3). The analysis reveals that as the entry angle η increases, the horizontal resultant force *Fxa* decreases, reducing the tooth's tendency to move forward at initial contact with the stone. Therefore, the preferred sequence for selecting tooth types is: forward-leaning, radial, and backward-leaning.

As shown in Figure 3b, a coordinate system is established with the center of the stone as the origin, where the direction perpendicular to the tooth contact surface serves as the *x*-axis and parallel to it serves as the *y*-axis. At the moment the tooth lifts the stone off the ground, no force is exerted on the stone by the ground. At this instant, the velocity in the direction perpendicular to the tooth contact surface is determined by the resultant force in that direction. The expression for the vertical resultant force acting on the working surface of the tooth is as follows:

$$F_{xb} = N_1 - G \sin\delta \quad (4)$$

where:

F_{xb} is the resultant force of the tooth in the direction perpendicular to the contact surface, [N]; δ is the angle of extraction from the soil, [°].

The derivative of equation (4) yields:

$$F'_{xb} = -G \cos\delta \quad (5)$$

where:

$$\delta < \pi/2 \quad (6)$$

Analysis of equations (5) to (6) reveals that as the extraction angle increases, the horizontal resultant force along the x-axis decreases, resulting in a reduced tendency for the stone to be lifted off the ground and diminishing the effectiveness of stone picking. When lifting the stone off the ground, the preferred sequence for selecting tooth types is: backward-leaning, radial, and forward-leaning teeth.

Balancing overall performance, radial teeth excel in continuously moving stones forward compared to backward-leaning teeth and are more effective in lifting stones off the ground than forward-leaning teeth. Therefore, selecting radial teeth maintains the stability of stone picking operations and can enhance the operational efficiency of the stone picker.

To facilitate the replacement of worn teeth, the teeth are designed to be detachable. The base of each tooth is curved to match the spiral blade roller, which enhances operational stability. To reduce soil resistance against the teeth, they are designed with a trapezoidal shape and sharpened tips. As shown in Fig. 4, the sharpened teeth have a reduced contact area at the tip, which lowers resistance during soil entry, enhances penetration ability, and reduces energy loss during contact *(Gao et al., 2023)*. When the tooth lifts the stone from the ground, the sharpened teeth cause the stone's weight and the angle of contact along the surface to decrease. Analysis of equations (5) and (6) shows that the sharpened teeth enhance the tendency to lift the stone off the ground along the tooth's vertical contact surface, thereby improving the stone-throwing effect.

The depth of stone extraction in farmland typically ranges from 0 to 50 mm below the surface; therefore, the chosen penetration depth for the teeth is set at 55 mm. The average profile length of stones is about 90 mm. To avoid excessive torque and power consumption from overly long teeth and inadequate stone-picking performance from overly short teeth, the length of the teeth is set at 140 mm. The diameter of the spiral blade roller is determined based on factors such as depth of penetration, size, and arrangement of the teeth. Considering all factors, the working diameter of the teeth (D) is set at 430 mm, while the diameter of the spiral blade roller (d) is 75 mm.

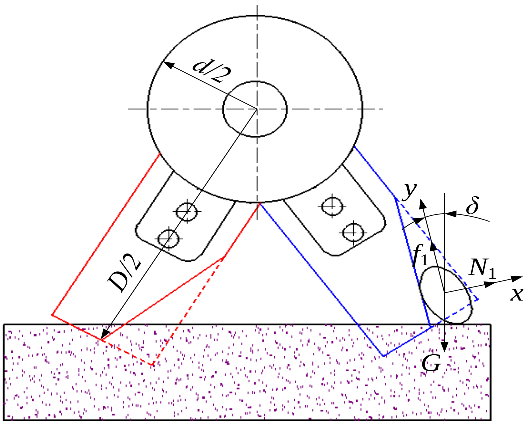

Fig. 4 - Comparison of tooth design before and after optimization

Design of tooth arrangement

An appropriate tooth arrangement can significantly enhance the stone-picking rate of the machine and reduce the occurrence of missed stones. Drawing on the principles of spiral cover implements *(Zheng et al., 2021;Yang et al., 2023)*, the teeth are arranged in a spiral pattern. Increasing the number of spiral lines reduces the rotational speed of the spiral blade roller, which decreases the velocity and kinetic energy exerted on the stones, thus reducing their tendency to be thrown from the ground. To avoid issues such as excessively high rotational speeds with a single spiral head, excessive power consumption, and poor stone-picking performance with multiple spiral heads, a dual spiral line arrangement is employed.

Stones with a maximum profile length exceeding 50 mm can adversely affect crop growth; therefore, the spacing between two adjacent teeth on the spiral blade roller is set at 50 mm, and the pitch is set at 800 mm. The spiral rise angle (α) is calculated using formula (7) to be 30.5°. The spiral blade rollers on the left and right sides are installed in opposite directions, forming a symmetrical structure. An illustrative diagram of tooth installation and arrangement is shown in Fig. 5.

$$\alpha = \arctan \frac{P}{\pi d} \tag{7}$$

where:

α is the angle of the spiral ascent, [°]; P is the pitch, [mm].

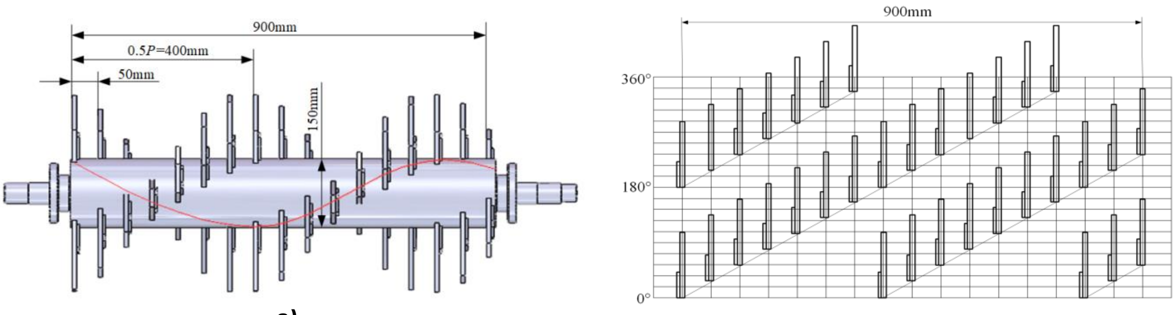

a) b)

Fig. 5 – Schematic diagram of tooth installation and arrangement
a) Tooth installation diagram; b) Double-helix arrangement diagram

Kinematic analysis of the tooth stone-picking process

When the stone picker moves at a uniform speed, the teeth rotate synchronously with the spiral blade roller. For analytical convenience, a spatial coordinate system O_{xyz} is established, as shown in Fig. 6. Here, the angle between the spiral blade roller and the *x*-axis is referred to as the side tilt angle γ. The *x*-axis indicates the direction of stone clearing, the *y*-axis is the forward direction of the equipment, and the *z*-axis is perpendicular to the ground. Using the centroid of the stone as the origin O_1 the component velocities of the tooth tip along the *x*, *y*, and *z* axes are as follows:

$$\begin{cases} v_x = R\omega \sin(\omega t) \sin\gamma \\ v_y = v_e + R\omega \sin(\omega t) \cos\gamma \\ v_z = R\omega \cos(\omega t) \end{cases} \tag{8}$$

where:

$$\omega = 2\pi n/60 \tag{9}$$

v_e is the forward speed of the machinery, [m/s]; ω is the angular velocity of the spiral cutting roller, [rad/s];
n is the rotational speed of the spiral cutting roller, [r/min]; R is the radius of rotation of the tooth, [mm];
γ is the inclination angle of the spiral cutting roller, [°].

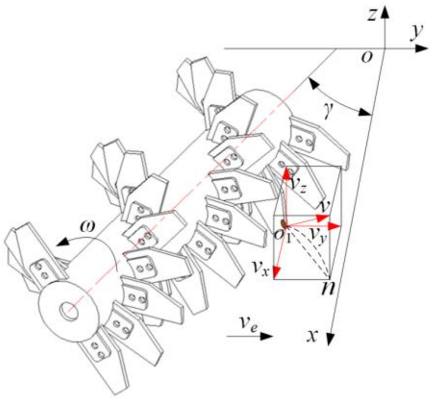

Fig. 6 – Kinematic analysis of the tooth

In the coordinate system O_{1xyz}, the absolute velocity of the tooth tip can be derived from equation (8):

$$|v| = \sqrt{v_x^2 + v_y^2 + v_z^2} = \sqrt{v_e^2 + R^2\omega^2 + 2v_e R\omega \sin(\omega t)\cos\gamma} \tag{10}$$

Based on equations (8) to (10), the factors affecting the absolute velocity of the tooth include the forward speed of the equipment v_e, the rotational speed of the spiral blade roller n, and the side tilt angle γ of the spiral blade roller. When the side tilt angle γ exceeds 45°, the lateral force on the tooth increases, making it prone to bending and damage, which reduces the effectiveness of the stone-picking operation. Therefore, the side tilt angle γ should be less than 45°. Since the lateral velocity v_{xy} and the dislodging velocity v_{yz} of the tooth directly affect the stone dislodgement distance and the soil disturbance coefficient *(Yao et al., 2022)*, the range for the side tilt angle γ is chosen to be between 20° and 40°. The operational process must ensure that the absolute velocity of the tooth is greater than the forward speed of the equipment v_e. The field operational speed of the stone picker v_e is set between 0.1 and 0.5 m/s. Through pre-experimental analysis, it was found that the stone-picking effect is optimal when the rotational speed n of the spiral blade roller is between 150 and 350 r/min.

Discrete element simulation analysis

EDEM simulation modeling

Establishing a realistic stone model is crucial for ensuring the accuracy of simulation data. Stones found in fields are typically rod-shaped, block-shaped, or slab-shaped, with particle sizes related to their shapes and contour lengths. Based on data from basic soil and stone experiments, stone particles are modeled using multi-sphere representations in the discrete element software. The average profile length is set at 90.0 mm, with stone sizes ranging from 50.0 mm to 120.0 mm. The size distribution parameter settings vary from 0.56 to 1.30, with a representative stone model illustrated in Fig. 7.

Fig. 7 – Discrete element model of the stone

During the operation of the stone picker, various contacts occur among tooth-soil particles, tooth-stone particles, soil-soil particles, soil-stone particles, and stone-stone particles. By combining initial parameter calibration with relevant literature, the physical and mechanical parameters of materials and the contact coefficients are determined *(Deng et al., 2022; Chen et al., 2024; Hao et al., 2023)*. The mechanical characteristic parameters for each material particle, along with the contact coefficients for other objects, are detailed in Tables 2 and 3. The simulation models for soil-soil and soil-stone contacts are based on the Hertz-Mindlin with JKR model, while the Hertz-Mindlin (no slip) model is used for other contact types *(Li et al., 2022; Shi et al., 2024; Zhang et al., 2022)*.

Table 2

Physical and mechanical parameters

Item	Soil particle	Stone	Tooth
Poisson's ratio	0.35	0.3	0.3
Density/kg·m^{-3}	2600	1600	7865
Shear modulus/Pa	2.5×10^7	1×10^7	7.9×10^{10}

Table 3

Material contact parameters

Item	Parameter	Value
Soil -Soil	Coefficient of restitution	0.5
	Static friction coefficient	0.8
	Dynamic friction coefficient	0.23
	Surface energy/(J·m^{-2})	5.5
Soil -Stone	Coefficient of restitution	0.06
	Static friction coefficient	0.5
	Dynamic friction coefficient	0.01
	Surface energy/(J·m^{-2})	5.5
Soil -Tooth	Coefficient of restitution	0.2
	Static friction coefficient	0.3
	Dynamic friction coefficient	0.25
Stone-Stone	Coefficient of restitution	0.3
	Static friction coefficient	0.5
	Dynamic friction coefficient	0.01

Item	Parameter	Value
Stone-Tooth	Coefficient of restitution	0.2
	Static friction coefficient	0.5
	Dynamic friction coefficient	0.01

To simplify the EDEM simulation computation and considering the symmetry of the entire machine with no mutual influence, the simulation focuses solely on one side. The length of the single spiral blade roller is reduced to 530 mm and features 0.65 turns. A virtual soil trough model is established with dimensions of 1500 mm (length) ×1100 mm (width) ×160 mm (height). Due to the large size of the soil trough, soil particles are modeled as single spheres with a radius of 5 mm, while stones are placed on the surface of the soil.

Simulation parameter settings

Using SolidWorks software, the model is created to scale and saved in .stp format for import into EDEM for preprocessing, as shown in Fig. 8. The spatial coordinates of the initial motion state are aligned with those of the soil trough model. The penetration depth is set to 55 mm, along with the correct rotation direction, angular velocity, machine advance direction, and forward speed. Based on the forward speed, the simulation time is set, with a mixing timestep of 20% and a target save interval of 0.01 s.

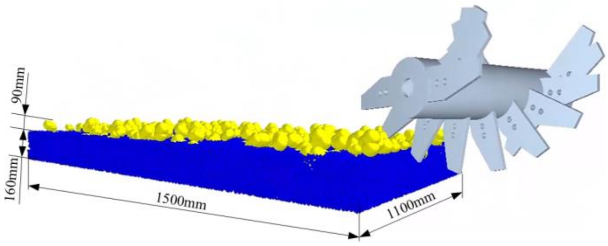

Fig. 8 – Modelling of stone-soil-knife-tooth interactions

Experimental design and methods

The method employed is a three-factor, five-level second-order regression orthogonal rotation central composite design. The experimental factors include the machine's forward speed, the rotational speed of the spiral blade roller, and the side tilt angle of the spiral blade roller, with the stone-picking rate and power consumption as the experimental indicators. The coding of the experimental factors is presented in Table 4.

Table 4

Experimental factors and codes

Coded Values	Factors		
	Forward speed/（m·s^{-1}）	Roller speed/（r·min^{-1}）	Roller side tilt angle/（°）
1.682	0.5	350	40
1	0.42	321	36
0	0.3	250	30
-1	0.18	179	24
-1.682	0.1	150	20

Determination of Stone-Picking Rate: The stone-picking rate Y_1 is calculated using the Selection module in EDEM's post-processing analysis options. This module outputs the number of stones within the grid area before and after operation, as illustrated in Fig. 9. The formula for calculating the stone-picking rate Y_1 is as follows:

$$Y_1 = \left(1 - \frac{W_1}{W}\right) \times 100\% \tag{11}$$

where: W is the number of rocks in the soil trench before operation; W_1 is the number of rocks missed in the soil trench after operation.

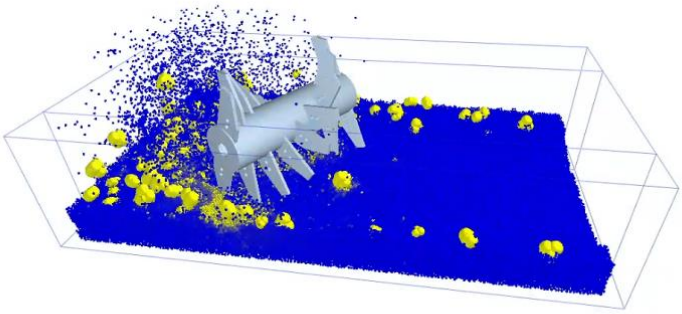

Fig. 9 – Simulation of the stone picker's operational process

Determination of Power Consumption: After the simulation is complete, torque data is exported using the EDEM post-processing module. The power consumption Y_2 of the spiral blade roller is calculated using the following formula:

$$Y_2 = P = \frac{T \times n}{9550} \tag{12}$$

where:

P is consumed power [kW]; T is the average torque of the spiral knife roller during operation [N·m].

Soil trough experiment

To validate the accuracy of the discrete element simulation results and the performance of the optimized stone picker, an indoor soil trough experiment was conducted on August 1, 2024, at the Key Laboratory of Intelligent Equipment at Xinjiang Agricultural University. The equipment used included the TCC-III computer-monitored soil trough test vehicle, stones, the spiral tooth-type stone picker, and a measuring tape.

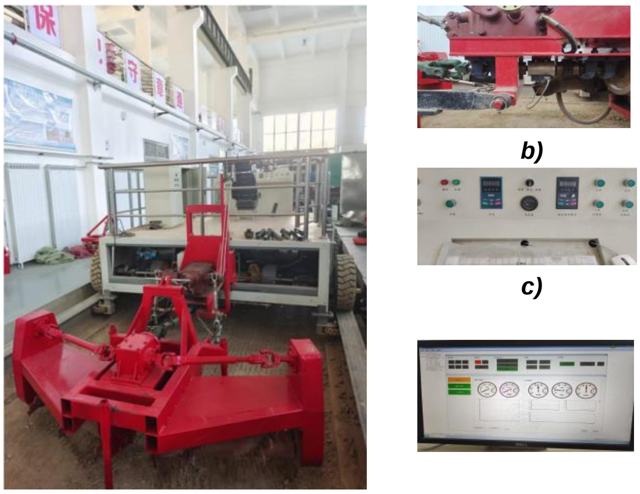

b)

c)

a) *d)*

Fig. 10 – Soil trench test

a) Experimental prototype; b) Power monitoring sensor; c) Parameter adjustment system; b) Data monitoring system

The equipment was connected to the soil trough test vehicle via a three-point hitch. The experimental setup is shown in Fig. 10. The trough contained original sandy soil, with stones randomly placed on the 2m×10m soil surface before operation. Soil moisture and compaction were measured using a soil moisture meter and a soil compaction tester. The results indicated a soil moisture content of 12.7% and a compaction of 4094.57 kPa. Based on the simulation results, the experimental conditions were set as follows: roller speed n=260 r/min, forward speed v_e=0.18m/s, tilt angle of 30°, and a working depth of 55 mm for a travel distance of 10 m in the soil trough.

RESULTS

Analysis of simulation experiment results

A total of 20 experiments were conducted, with the results presented in Table 5, where X_1, X_2 and X_3 represent the coded values of the experimental factors.

Table 5

Experimental design and results

Test No.	Factors			Response Value	
	X_1	X_2	X_3	Y_1/%	Y_2/%
1	-1	-1	-1	87.27	2.17
2	1	-1	-1	84.46	3.44
3	-1	1	-1	93.31	4.03
4	1	1	-1	86.67	5.99
5	-1	-1	1	90.26	3.81
6	1	-1	1	87.54	4.91
7	-1	1	1	96.67	6.24
8	1	1	1	89.21	8.19
9	-1.682	0	0	96.88	3.06
10	1.682	0	0	88.02	5.67
11	0	-1.682	0	85.56	4.21
12	0	1.682	0	95.23	8.42
13	0	0	-1.682	86.15	3.18
14	0	0	1.682	92.74	6.24
15	0	0	0	91.21	3.64
16	0	0	0	92.84	3.79
17	0	0	0	92.31	3.81
18	0	0	0	92.57	3.78
19	0	0	0	93.66	3.45
20	0	0	0	93.27	3.92

The experimental data were processed using Design-Expert 13.0 to perform regression analysis and significance testing on the simulation results. Based on the analysis of variance (ANOVA), model significance, lack of fit, and correlation were evaluated, with results presented in Table 6. The ANOVA results indicate that both regression models for the stone-picking rate and power consumption are significant (P< 0.01), while lack-of-fit terms are non-significant (P>0.05), demonstrating a good fit of the regression model equations. Thus, these models can be effectively used for the analysis and optimization of the experimental indicators. The order of influence of each factor on the stone-picking rate is as follows: machine forward speed, spiral blade roller rotational speed, and side tilt angle. For power consumption, the order of influence is: spiral blade roller rotational speed, side tilt angle, and machine forward speed. An F-test at a 0.05 confidence level was conducted, with non-significant terms removed to obtain the final regression model as follows:

$$\begin{cases} Y_1 = 92.68 - 2.53X_1 + 2.39X_2 + 1.69X_3 - 1.07X_1X_2 - 0.33X_1^2 - 1.05X_2^2 - 1.39X_3^2 \\ Y_2 = 3.74 + 0.78X_1 + 1.26X_2 + 0.93X_3 + 0.19X_1X_2 + 0.15X_1^2 + 0.84X_2^2 + 0.27X_3^2 \end{cases} \tag{13}$$

Table 6

Results of the ANOVA

Index	Variation source	Sum of squares	Degrees of freedom	Mean Square	F	P
Y_1	Model	253.45	9	28.16	24.16	<0.0001**
	X_1	87.31	1	87.31	74.90	<0.0001**
	X_2	77.79	1	77.79	66.73	<0.0001**
	X_3	38.91	1	38.91	33.38	0.0002**
	X_1X_2	9.18	1	9.18	7.88	0.0186*
	X_1X_3	0.067	1	0.067	0.057	0.8159
	X_2X_3	3.6×10^{-3}	1	3.6×10^{-3}	3.1×10^{-3}	0.9567
	X_1^2	1.54	1	1.54	1.32	0.2770

Index	Variation source	Sum of squares	Degrees of freedom	Mean Square	*F*	*P*
	X_2^2	16.00	1	16.00	13.72	0.0041**
	X_3^2	27.82	1	27.82	23.86	0.0006**
	Residual	11.66	10	1.17		
	Lack of fit	8.02	5	1.60	2.21	0.2028#
	Error	3.64	5	0.73		
	Total	265.10	19			
Y_2	Model	52.86	9	5.87	102.48	<0.0001**
	X_1	8.34	1	8.34	145.45	<0.0001**
	X_2	21.66	1	21.66	378.00	<0.0001**
	X_3	11.75	1	11.75	204.98	<0.0001**
	X_1X_2	0.30	1	0.30	5.17	0.0462*
	X_1X_3	4.0×10^{-3}	1	4.0×10^{-3}	0.071	0.7958
	X_2X_3	0.21	1	0.21	3.69	0.0838
	X_1^2	0.31	1	0.31	5.39	0.0427*
	X_2^2	10.07	1	10.07	175.68	<0.0001**
	X_3^2	1.04	1	1.04	18.11	0.0017**
	Residual	0.57	10	0.057		
	Lack of fit	0.44	5	0.088	3.24	0.1113#
	Error	0.14	2	0.027		
	Total	53.43	19			

*Note: **means extremely significant impact ($P<0.01$), *means significant impact($0.01\leq P<0.05$), # means no significant impact ($P > 0.05$).*

Response surfaces were created to illustrate the effects of interactions among factors on the stone-picking rate and power consumption. Fig. 11a shows that, at a central level of the spiral blade roller's side tilt angle, the stone-picking rate is positively correlated with both the forward speed and the rotational speed of the spiral blade roller. When the roller's rotational speed is constant, an increase in forward speed results in a decrease in the lateral push speed of the tooth, which may prevent stones from being directed to one side within a limited distance. This increases the likelihood of missed stones and reduces the picking rate. Conversely, at a constant forward speed, increasing the roller speed enhances the lateral displacement of the stones and the frequency of stone lifting per unit time, thereby increasing the stone-picking rate.

Fig.11b indicates that, at a central tilt angle and constant forward speed, power consumption initially decreases and then increases with an increase in roller speed. Excessively high roller speeds lead to more frequent stone-lifting events, which ultimately increases power consumption. When the roller speed is constant, power consumption rises with increasing forward speed due to the increased contact distance between the teeth and the soil, which heightens resistance and increases operational torque. Increased power consumption reduces the lifespan of the teeth and raises strength requirements. To enhance stone-picking efficiency while minimizing power consumption, the structural and operational parameters of the equipment should be optimized.

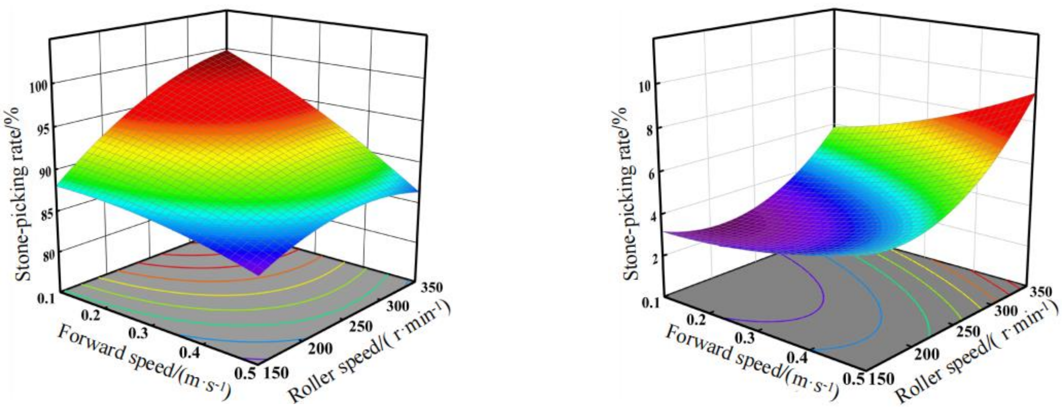

a) *b)*

Fig. 11 – Response surface of the effect of factor interactions on each indicator

a) Effect of interaction factors on the stone-picking rate; b) Effect of interaction factors on power consumption

Parameter optimization

To achieve optimal performance, the Optimization module of Design-Expert software was used to perform constrained optimization of the regression model. The aim was to maximize stone-picking efficiency while minimizing power consumption. The objective function and constraints were defined as follows:

$$\begin{cases} \max Y_1(X_1, X_2, X_3) \\ \min Y_2(X_1, X_2, X_3) \\ \text{s.t.} \begin{cases} -1.682 \le X_1 \le 1.682 \\ -1.682 \le X_2 \le 1.682 \\ -1.682 \le X_3 \le 1.682 \end{cases} \end{cases} \tag{14}$$

When analyzing simulation parameters in the optimization module, the importance levels for the evaluation indicators were set, prioritizing the stone-picking rate as "+++" and power consumption as "++." The optimal parameter combination obtained was a forward speed of 0.18 m/s, a spiral blade roller speed of 274.71 r/min, and a side tilt angle of 30.28°. To account for the difficulty of setting exact speed ratios in the machine, the roller speed was rounded to 260 r/min and the tilt angle to 30°.

Analysis of the results of the soil trough experiment

Stone-picking rate measurement

The experiment included five repeat tests, with the average value taken as the verification result. The soil trough experiment setup is shown in Fig. 12. When operating under the optimal parameter combination, the average stone-picking rate achieved was 93.71%, with a deviation of 3.2% from the theoretical value. This indicates a close alignment between the experimental results and the model predictions. This outcome demonstrates that the designed stone picker performs well and meets the requirements for farmland stone-picking operations.

Fig. 12 – Prototype operation effect

Power consumption measurement

Once the equipment achieved stable operation, sensors recorded the real-time rotational speed and torque of the soil trough test vehicle's output shaft. A dynamic torque sensor transmitted the torque data in real time to the digital display. Torque data for the 2–4 second interval is shown in Fig.13.

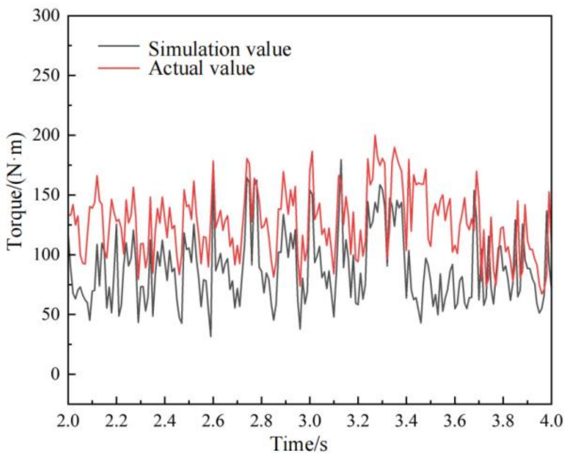

Fig. 14 – Power consumption verification

The average power consumption of the spiral blade roller was calculated using the torque formula. The average operational power consumption was 4.63 kW, which is slightly higher than the theoretical value. This discrepancy is likely due to the complex actual operating environment, the lower real speed compared to the theoretical speed, and the presence of numerous small stones.

CONCLUSIONS

（1）In response to the low stone-picking rate and high power consumption of existing stone pickers, a spiral tooth-type farmland stone picker was designed. A mechanical analysis of different tooth shapes for stone picking identified the optimal tooth type, followed by structural optimization of the teeth. A kinematic analysis of the stone-lifting process was conducted to establish the structural and operational parameters of the main components.

（2）Using EDEM discrete element simulation software, an interaction model among stones, soil, and teeth was developed. A three-factor, five-level, second-order regression orthogonal rotation central composite design was employed, with machine forward speed, spiral blade roller speed, and side tilt angle as factors, and stone-picking rate and power consumption as performance indicators. The effects of factor interactions on these performance indicators were analyzed.

（3）Design-Expert software was utilized to optimize the operating parameters of the stone picker. Optimal performance was achieved at a forward speed of 0.18 m/s, a spiral blade roller speed of 260 r/min, and a side tilt angle of 30°. Under these optimized conditions, the soil trough test demonstrated an average stone-picking rate of 93.71% and a power consumption of 4.63 kW. The spiral tooth-type stone picker exhibited stable operational performance, providing valuable insights and a reference framework for future optimization and design improvements of stone-picking machines.

ACKNOWLEDGEMENT

The authors were funded for this project by the Natural Science Foundation of Xinjiang Uygur Autonomous Region (Grant NO.2022D01A245).

REFERENCES

[1] Chengzhi Deng, Shanwen Wang, Zhanpeng Li, Chong Chen, Zhiqiang Wei, Tingyi Duan. (2022). Optimization analysis of operation parameters of home plate in soil based on the discrete element method *(基于离散元法的锄板入土作业参数优化分析)*. *Journal of Chinese Agricultural Mechanization*, Vol. 43, no.07, pp.188-196, Chongqing/China.

[2] Chong Zhang, Xuhui Fan, Mingsen Li, Guang Li, Chunkai Zhao, Wenliang Sun. (2022). Simulation analysis and experiment of soil disturbance by chisel plow based on EDEM *(基于 EDEM 的凿式犁铲土壤扰动仿真分析与试验)*. *Transactions of the Chinese Society for Agricultural Machinery*, Vol.53, no.S2, pp.52-59, Jilin/China.

[3] Cong Niu, Yuting Xing, Chenggong Yan, Haochao Tan, Shuai Ma, Liming Xu. (2022). Simulation and experiment of shovel-screen type farmland stone picking and collecting machine *(铲筛式农田石块捡拾收集机仿真与试验)*. *Journal of China Agricultural University*, Vol. 27, no.12, pp.221-233, Beijing/China.

[4] Fang Ma, Lianxing Gao, Yuzhen Yu. (2007). Research on selecting picking equipment of surface harrow type rack rail rock picker's mechanism and parts *(轮齿式浅耙型农田捡石机分捡装置研究)*. *Journal of Agricultural Mechanization Research*, no.5, pp.115-117, Shenyang/China.

[5] Jia Zhang, Hong Wang, Chuanjiang Li, Jiaxi Zhang, Yakun Du. (2024). Analysis on the development trend of farmland soil stone-picking mechanization technology based on patent bibliometrics *(基于专利计量的农田土壤捡石机械化技术发展态势分析)*. *Journal of Chinese Agricultural Mechanization*, Vol.45, no.6, pp.250-256, Xinjiang/China.

[6] Jicheng Li, Kunpeng Sun, Yonghua Zhang, Tianhui Zhang. (2023). Simulation of tillage behavior of double winged subsoiler based on discrete element method *(基于离散元法的双翼深松铲耕作行为的仿真分析)*. *Journal of Inner Mongolia Agricultural University (Natural Science Edition)*, Vol.44, no.2, pp.67-75, Yunnan/China.

[7] Kang Zheng, Yufei Li, Junfang Xia, Guoyang Liu, Jian Cheng, Qixin Kang. (2021). Design and experiment of land leveling blade roller of ditching and rotary tiller with gradual spiral angle *(开沟旋耕机渐变螺旋升角轴向匀土刀辊设计与试验)*. *Transactions of the Chinese Society for Agricultural Machinery*, Vol.52, no.1, pp.63-73, Hubei/China.

[8] Linrong Shi, Wuyun Zhao, Wei Sun. (2017). Parameter calibration of soil particles contact model of farmland soil in northwest arid region based on discrete element method *(基于离散元的西北旱区农田土壤颗粒接触模型和参数标定)*. *Transactions of the Chinese Society of Agricultural Engineering (Transactions of the CSAE)*, Vol.33, no.21, pp.181-187, Gansu/China.

[9] Mingjie Bu, Yangli Liu, Yuan Xu, Feng Wang, Yuchen Liu, Fengwei Zhang. (2022). Design and test of chain stone picker for reclaiming farmland *(复垦农田链式捡石机的设计与试验)*. *Agricultural Equipment & Vehicle Engineering*, Vol.60, no.10, pp.31-35+41, Beijing/China.

[10] Shengquan Li, Xiaogang Liu, Dongliang Li. (2024). Dynamic modeling and simulation of stress for farmland rock picker based on dynamic analysis *(基于动力学分析的农田捡石机应力动态建模与仿真)*. *China Southern Agricultural Machinery*, Vol.55, no.11, pp.24-27, Gansu/China.

[11] Weixiang Chen, Jibiao Qin, Chongcheng Chen, Yang Liu, Shuhe Zheng. (2024). Design and parameter optimization of trenching and soil-throwing blade for ecological tea garden by discrete element method (*基于离散元法的生态茶园开沟抛土刀设计与参数优化)*. Journal of Fujian *Agriculture and Forestry University (Natural Science Edition)*, Vol. 53, no.1, pp.136-144, Fujian/China.

[12] Wenwu Yang, Xiwen Luo, Zaiman Wang, Minghua Zhang, Shan Zeng, Ying Zang. (2016). Design and experiment of track filling assembly mounted on wheeled-tractor for paddy fields *(轮式拖拉机水田轮辙覆土装置设计与试验)*. *Transactions of the Chinese Society of Agricultural Engineering (Transactions of the CSAE)*, Vol. 32, no.16, pp.26-31, Guangdong/China.

[13] Wenyan Yao, Dianbao Zhao, Hequan Miao, Peide Cui, Maojian Wei, Peisong Diao. (2022). Design and experiment of oblique anti-blocking device for no-tillage planter with shallow plowing stubble clearing (*免耕播种机浅旋清茬斜置式防堵装置设计与试验)*. *Transactions of the Chinese Society for Agricultural Machinery*, Vol. 53, no.8, pp.42-52, Shandong/China.

[14] Xiaomei Zhan, Yali Li, Zhonghua Cao, Qinghui Yang, Jinbo Cui. (2023). Design of 1JS-100 soil stone picker *(1JS-100 土壤捡石机的设计)*. *Journal of Agricultural Mechanization Research*, Vol.45, no.8, pp. 69-73, Chongqing/China.

[15] Yuzhen Yu, Yucai Zheng, Lianxing Gao, Fang Ma. (2007). Kinematics analysis on chain tooth rock picker in the farmland soil *(农田捡石机捡石机理研究)*. *Journal of Agricultural Mechanization Research*, no.3, pp.49-51, Hebei/China.

[16] Yuzhen Yu, Lianxing Gao, Xinping Li, Fang Ma. (2007). Study of rock picker in farmland and the mechanism of rock picking *(链齿式农田土壤捡石机栅条齿动力学分析)*. *Journal of Agricultural Mechanization Research*, no.5, pp.210-211, Hebei/China.

[17] Yuzhen Yu, Lianxing Gao, Xiuli Ma, Fang Ma, Jinsheng Zhao. (2007). Research advance in the development of soil rock picker *(土壤捡石机的研究进展)*. *Transactions of the Chinese Society of Agricultural Engineering (Transactions of the CSAE)*, no.11, pp. 274-279, Hebei/China.

[18] Zhen Gao, Caiyun Lu, Xuyang Wei, Hongwen Li, Jin He, Qingjie Wang. (2023). Design and experiment of co-stirring combined corn strip straw cleaning device *(协拨组合式玉米条带秸秆清理装置设计与试验)*. *Transactions of the Chinese Society for Agricultural Machinery.* Vol.54, no.10, pp.68-79, Beijing/China.

[19] Zhihao Hao, Enlai Zheng, Xun Li, Haoping Yao, Xiaochang Wang, Shengyue Qian, Weixun Li, Min Zhu. (2023). Performance analysis of the soil-contacting parts for no-tillage planters and optimization of blade structure *(免耕播种机旋耕刀耕作性能分析与结构优化)*. *Transactions of the Chinese Society of Agricultural Engineering (Transactions of the CSAE)*, Vol.39, no.2, pp.1-13, Jiangsu/China.